Journal of Alloys and Compounds 509 (2011) 7900–7908

Contents lists available at ScienceDirect

Journal of Alloys and Compounds

journal homepage: www.elsevier.com/locate/jallcom

Photoluminescence and optical properties of nanostructure Ni doped ZnO thin films prepared by sol–gel spin coating technique

A.A.M. Farag[a], M. Cavaş[b], F. Yakuphanoglu[c,*], F.M. Amanullah[d]

[a] Thin Film Laboratory, Physics Department, Faculty of Education, Ain Shams University, Cairo, Egypt
[b] Elbistan Higher Vocational School, Kahramanmaraş Sütçü İmam University, Elbistan, Turkey
[c] Department of Metallurgical and Materials Engineering, Fırat University, Elazığ, Turkey
[d] Department of Physics and Astronomy, College of Science, King Saud University, Riyadh, Saudi Arabia

ARTICLE INFO

Article history:
Received 22 February 2011
Received in revised form 2 May 2011
Accepted 3 May 2011
Available online 11 May 2011

Keywords:
Ni-doped ZnO
Nanostructure thin film
Optical constants
Sol–gel
Spin coating

ABSTRACT

In this work, the spin coating sol–gel technique has been successfully used to deposit highly uniform and good adhesion of nano structure thin films of ZnO doped with different Ni concentrations. The morphological properties of ZnO:Ni films were studied by atomic force microscopy (AFM) technique. The surface morphology of the nanostructure films is found to depend on the concentration of Ni. The effects of Ni contents on the structural and photoluminescence (PL) properties of ZnO films were investigated. Optical constants (refractive index, n, and absorption index, k) of the undoped and Ni-doped ZnO of 0.2%, 0.4%, 0.6%, 0.8%, 1%, 3%, 5% and 7% concentrations have been obtained in the wavelength range 200–1000 nm by using spectrophotometric measurements. The dispersion parameters were determined and discussed based on the single oscillator model.

1. Introduction

Nanostructured materials have received much attention because of their novel properties, which differ from those of bulk materials [1–3]. Control of dimension and morphology of materials has aroused the interest of researchers in the design of functional devices due to the optical and electronic properties of nanometer- and micrometer-sized materials, which determine their applications adapted by varying their size and shape [4].

Zinc oxide (ZnO) which is a versatile semiconductor material, has been attracting attention because of the commercial demand for optoelectronic devices operating at blue and ultraviolet regions [5] and it is a wurtzite-type semiconductor with band gap energy of 3.37 eV and very large excitation binding energy (60 meV) at room temperature [6]. Recently, special attention has been devoted to the morphology of ZnO having various nanostructures [7,8]. Thermal stability, irradiation resistance and flexibility to form different nanostructures are the advantages that expedite its potential wide applications in photodetectors [9], surface acoustic wave devices [10], ultraviolet nanolaser [11], varistors [12], solar cells [13], gas sensors [14], biosensors [15], ceramics [16], field emission [17], and nanogenerator [18].

At present, ZnO nanoparticles have received considerable attention due to their unique properties [19]. They are well known as UV blocking materials, especially of light in the UV region, and as such are used widely in cosmetics, paints and fibers, but their high catalytic activity in oxidation and photochemical reactions restrict their application as UV blocking materials. Particle surface modification is regarded as an effective way to restrain the ultra-fine particles high oxidative and photochemical catalytic activities [20].

It is well known that the addition of impurities into a wide gap semiconductor, such as ZnO can often induce dramatic changes in the optical, electrical, and magnetic properties [21–23]. Therefore, a selective doping element into ZnO has become an important route for enhancing and controlling its optical, electrical, and magnetic performance, which are crucial for their practical applications [23].

It was reported that transition-metal (TM)-doped ZnO materials would be a good candidate to achieve Curie temperature above room temperature [24,25], and great efforts have been devoted to the investigation of magnetic-metal/ZnO materials [26–29]. Ni is an important dopant in the magnetic materials. Furthermore Ni^{2+} (0.69 Å) has the same valence compared to Zn^{2+} and its radius is close to Zn^{2+} (0.74 Å), so it is possible for Ni^{2+} to replace Zn^{2+} in ZnO lattice. Some researches on Ni doped ZnO have been reported and several results showed that the luminescence properties of ZnO were changed after doping of Ni [30–33]. By doping Ni into ZnO, a composite material with magnetic and optical properties could be obtained. Although several experimental studies have been reported on the structural, morphological, electrical and opti-

* Corresponding author. Tel.: +90 424 2370000x3621; fax: +90 424 2330062.
E-mail address: fyhanoglu@firat.edu.tr (F. Yakuphanoglu).

0925-8388/$ – see front matter © 2011 Elsevier B.V. All rights reserved.
doi:10.1016/j.jallcom.2011.05.009

cal properties of nickel-doped ZnO nanostructured films, there are few reports on the optical constants of them in the available literature. In this paper, we report the influence of Ni doping on the structural, morphological, optical and electrical properties of sol–gel derived ZnO film. In this paper, we successfully synthesized Ni-doped ZnO nano-structure films have a fiber network with uniform using a simple sol–gel spin coating method with controlling Ni contents. This method may be used for preparation of many new device materials in microscale electronics and photonics such as novel memory and optical device, and it will be applied in biological detecting and treatment. ZnO fiber network nanostructure with various microstructure parameters can be controlled by changing the concentrations of the dopants. Moreover, the effect of Ni doping concentration on the optical characteristics of sol–gel derived ZnO film was considered.

2. Experimental procedures

2.1. Materials and preparation

The zinc acetate dehydrate [$Zn(CH_3CO_2)_2{\cdot}2H_2O$; ZnAc] and nickel acetate dehydrate [$Ni(CH_3CO_2)_2{\cdot}2H_2O$; NiAc] were used for preparation of ZnO films. 2-Methoxethanol and monoethanolamine (MEA) were used as the solvent and stabilizer, respectively. The molar ratio of MEA to ZnAc was maintained at 1.0 and the concentration of ZnAc and NiAc was 1 M. ZnAc and NiAc solutions were mixed together in Ni/Zn nominal molar proportions 0.2%, 0.4%, 0.6%, 0.8%, 1%, 3%, 5% and 7%. The solutions were stirred at room temperature for 2 h to yield a clear and homogeneous solution. The glass substrates were cleaned in methanol and acetone for 10 min each by using an ultrasonic cleaner and then cleaned with deionized water and dried. The coating solution was dropped onto a glass substrate, which was rotated at 2000 rpm for 30 s by using a spin coater. After the deposition by spin coating, the film was preheated at 200 °C for 10 min in a furnace to evaporate the solvent and remove organic residuals. The procedures from coating to drying were repeated ten times. The films were then inserted into a tube furnace and annealed in air at 400 °C for 1 h.

2.2. Measurements

The surface morphology of the prepared films was observed by atomic force microscopy, AFM (type Park System XE-100E). The photoluminescence (PL) spectra of the prepared films were recorded by a fluorescence spectrophotometer (LS 45) with an excitation wavelength of 325 nm. The measurements of the transmittance $T(\lambda)$ and reflectance $R(\lambda)$ were carried out using a double beam spectrophotometer model Shimadzu UV 2450 spectrophotometer with an integrating sphere in the wavelength range 200–1000 nm with step of 0.5 nm. All the measurements were carried out at room temperature.

2.3. Method of optical constants calculations

In order to calculate the optical constants, the spectrophotometric measurements of transmittance and reflectance were used. ZnO and nickel-doped ZnO thin films were deposited onto glass transparent substrates.

The absorption coefficient α is defined by the following relation [34]:

$$\alpha = \frac{1}{d}\ \ln\left(\frac{(1-R^2)}{2T} + \sqrt{\frac{(1-R)^4}{4T^2} + R^2}\right) \quad (1)$$

where $R(\lambda)$ is the reflectance and the relation between n and the absorption index k is given by the Fresnel formula as [35]:

$$R = \frac{(n-1)^2 + k^2}{(n+1)^2 + k^2} \quad (2)$$

where $k = \alpha\lambda/4\pi$. If one solves Eq. (2) via elementary algebraic manipulation, refractive index is obtained as:

$$n = \left(\frac{1+R}{1-R}\right) + \sqrt{\frac{4R}{(1-R)^2} - k^2} \quad (3)$$

When the film thickness is known, then the computation can be carried out and the optical constants can be calculated. The optical constants n and k were estimated by taking the consideration of the experimental errors in measuring the film thickness as ±2%, and $T(\lambda)$ and $R(\lambda)$ as ±1%.

3. Results and discussion

3.1. Surface morphological characterizations of the ZnO films

The surface morphology of the films was studied by using AFM. Fig. 1 shows AFM images of the ZnO and Ni-doped ZnO (0.2%, 0.4%, 0.6%, 0.8%, 1%, 3%, 5% and 7%). It is seen that the surface morphologies of the films are almost homogeneous. The connective and partially cylindrical structures may originate from the formation of sintering necks between former possible spherical particles. Furthermore, the AFM images indicate that all the films have a wrinkle network with uniform size distributions. The necks widths were influenced by the Ni content of 0.2%, 0.4%, 0.6%, 0.8%, 1%, 3%, 5% and 7% as shown in Fig. 1. The density of fiber network was found to decrease in the ZnO:7% Ni doped samples. The general observation for the AFM images is that the effect of Ni–doping concentrations has an important effect on the surface morphology of the film.

3.2. Photoluminescence characterization of the ZnO films

Features of the emission spectrum can be used to identify surface, interface, and impurity levels and to gauge alloy disorder and interface roughness. The intensity of the photoluminescence, PL signal provides information on the quality of surfaces and interfaces. Fig. 2 shows PL spectra of the ZnO and Ni-doped ZnO (0.2%, 0.4%, 0.6%, 0.8%, 1%, 3%, 5% and 7%) films. The origin of the emission band around 400 nm (3.10 eV) for all samples may be caused by the electron transition from the energy level of interstitial Zn to valance band [36–38]. This peak is highly intense in the spectrum of the undoped ZnO and ZnO with 0.2% and 0.8% Ni as compared to other samples. The observation of 400 nm peak in all samples likely indicates the existence of Zn interstitials in these sol–gel prepared ZnO nanostructures [39]. The low intensity of 400 nm peak in the 7% Ni-doped ZnO sample suggests that a low amount of interstitial Zn might be present in the nanostructures. The change in the Ni concentration of 0.4%, 0.6%, 1%, 3% and 5% has not a regular intensity which may be attributed to the change in the effect of both Zn interstitial and oxygen vacancies in the samples. This phenomenon gives an evidence for the suggestion of the role for the introduction of Ni to passivity or activates the Zn interstitials or the oxygen vacancies. The emission band around 530 nm (2.34 eV) for all samples has been frequently observed and may be attributed to the oxygen vacancies in ZnO [39].

3.3. Optical constant characterization of the ZnO films

The spectral distribution of $T(\lambda)$ and $R(\lambda)$ for the undoped ZnO and Ni-doped ZnO measured at the normal incidence in the wavelength range 200–1000 nm is shown in Figs. 3 and 4. It is clear from Fig. 3 that the all samples exhibit a high transmittance around >85% at $\lambda > 500$ nm. A sharp decrease in the transmittance is observed at about 370 nm attributed to the band edge absorption. This strong absorption means that the incoming photons have the sufficient energy to excite electrons from the valence band to the conduction band. Also, no remarkable dependence of the measured transmittance on the doping concentration of Ni in the studied range especially near the band edge was observed. The spectral behavior of the reflectance $R(\lambda)$ in Fig. 4 shows a dependence of the Ni doping. All the samples show a reflectance peak at about 400 nm accompanied with a sharp decrease in the reflectance in the spectral range 400–950 nm. After which in the spectral range 950–1150 nm, an increase in the reflectance comes again. In the spectral range of 850–1000 nm, the reflectance in all samples is almost slowly decreased.

To estimate the absorption band edge of the films, the first derivative of the optical transmittance can be computed. The curves

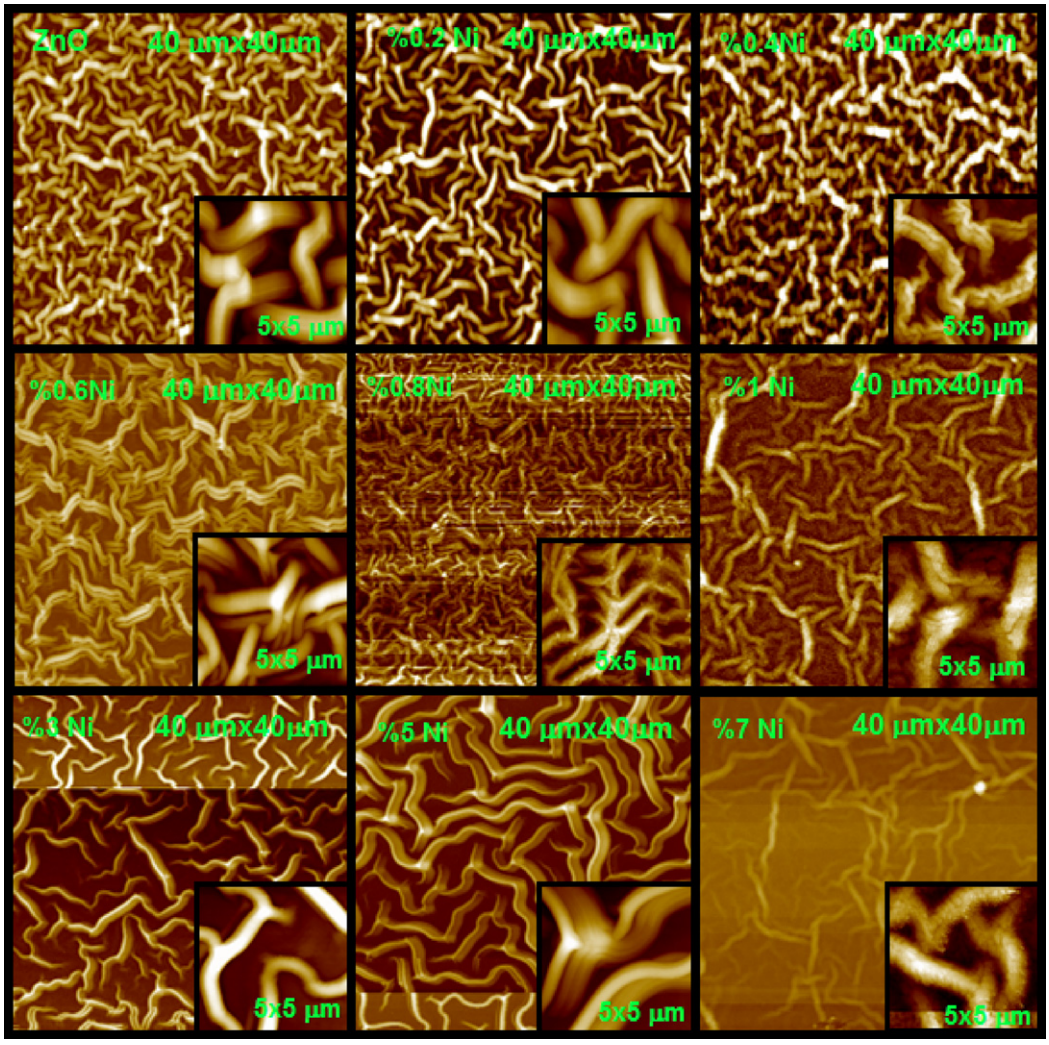

Fig. 1. AFM images of ZnO and ZnO doped with Ni of different concentrations.

of both $dT = d\lambda$ and $dR = d\lambda$ vs. wavelength were plotted, as shown in Fig. 5. As seen in these figures, the maximum peak position corresponds to the absorption band edge and it shifts to longer wavelengths. The maximum peak values are observed in the above two figures for the ZnO and Ni-doped ZnO films. This gives an evidence for the presence of the optical band gap which lies in the range 3.30–3.33 eV. Moreover, there is no remarkable effect was observed for the Ni dopant concentrations in the studied range on

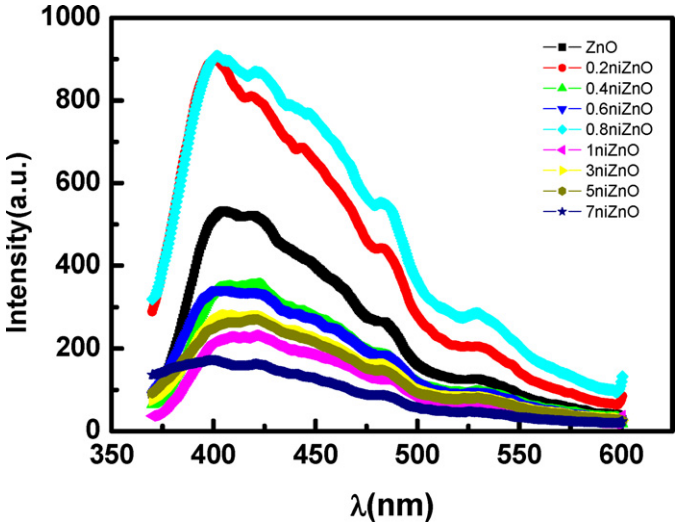

Fig. 2. Photoluminescence spectra of undoped ZnO and Ni-doped ZnO.

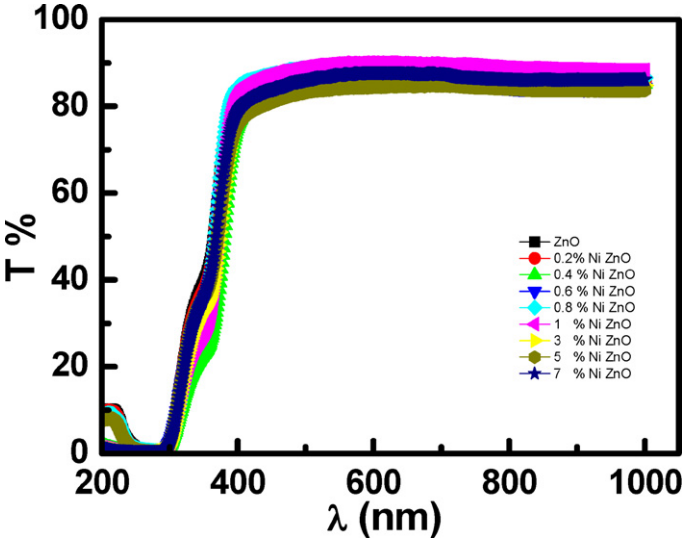

Fig. 3. Transmittance spectra of undoped ZnO and Ni-doped ZnO.

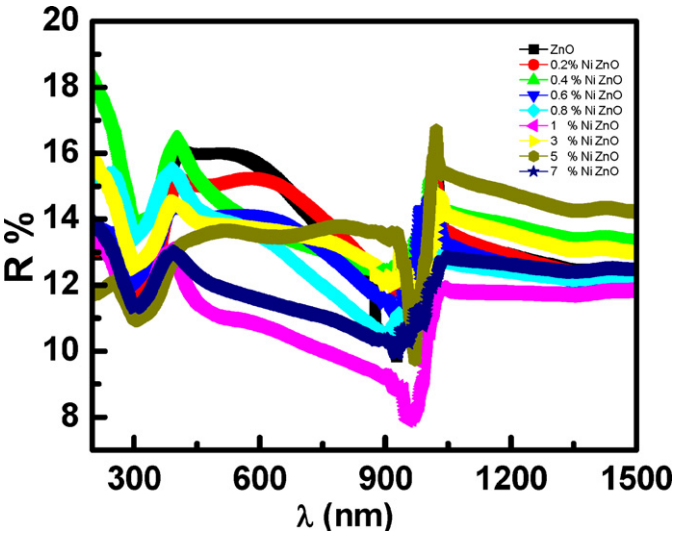

Fig. 4. Reflectance spectra of undoped ZnO and Ni-doped ZnO.

the optical band gap estimated from $dT/d\lambda$ vs. λ. In addition, there is an effect of the Ni dopant concentrations but not regular in the studied range on the optical band gap estimated from $dR/d\lambda$ vs. λ suggesting that the optical band gap shifts from 3.30 to 3.39 eV. The estimated energy gap from $dT/d\lambda$ and $dR/d\lambda$ ZnO and Ni-doped ZnO films is given in Table 1. It is well known that optical transitions can take place as direct or indirect transitions between the valence and conduction bands. Thus, we have evaluated that the exact value of the optical band gap with allowed direct transitions for the films as shown in the following subsection.

The refractive and absorption indices n and k of nanostructure ZnO and Ni-doped ZnO films were determined from the measured transmittance and reflectance at normal light incidence. The spectral dependences of both $n(\lambda)$ and $k(\lambda)$ are plotted in Fig. 6.

The absorption index k values for the films are very small at longer wavelengths, showing that the prepared films are highly transparent. The dispersion plays an important role in the research for optical materials due to a significant factor in optical communication and in designing devices for spectral dispersion [40]. The

Table 1
The values of energy gap for undoped and Ni-doped ZnO films.

	Function			
	$dT/d\lambda$ E_g (eV)	$dR/d\lambda$ E_g (eV)	$d(\alpha h\nu)/dh\nu$ E_g (eV)	$(\alpha h\nu)^2$ E_g (eV)
Ni content%				
0	3.28	3.39	3.34	3.31
0.2	3.30	3.38	3.34	3.33
0.4	3.34	3.37	3.33	3.33
0.6	3.32	3.36	3.35	3.29
0.8	3.35	3.39	3.33	3.33
1	3.34	3.40	3.32	3.33
3	3.35	3.39	3.33	3.30
5	3.34	3.29	3.34	3.33
7	3.39	3.45	3.33	3.30

evaluation of the refractive index of optical materials is considerably important for the applications in integrated optics devices, such as switches, filters and modulation, etc., in which the refractive index is a key parameter for the device design [41].

The refractive index n of ZnO and Ni-doped ZnO thin film shows an anomalous dispersion in the spectral range 340 <λ> 400 nm and 800 <λ> 855 nm. Moreover, the films show a normal dispersion in the spectral range 400 <λ>800 nm. The anomalous behavior is due to the resonance effect between the incident electromagnetic radiation and the electrons polarization, which leads to the coupling of electrons in ZnO films to the oscillating electric field. Moreover, the peak in the refractive index spectra corresponds to the fundamental energy gap of the ZnO film. This peak, n_{max} is slightly shifted towards long wavelength with increasing Ni%. The variation of the maximum refractive index for the undoped ZnO and Ni-doped ZnO films is shown in Fig. 7.

3.4. Optical absorption characterization of the ZnO films

In many semiconducting materials, it is usual to analyze the optical absorption at the fundamental edge in terms of band-to-band transitions theory [42,43]. In this treatment, the absorption data follow a power-law behavior of Tauc [44,45] given by

$$\alpha = \left(\frac{A}{h\nu}\right)(h\nu = E_g)^m \quad (4)$$

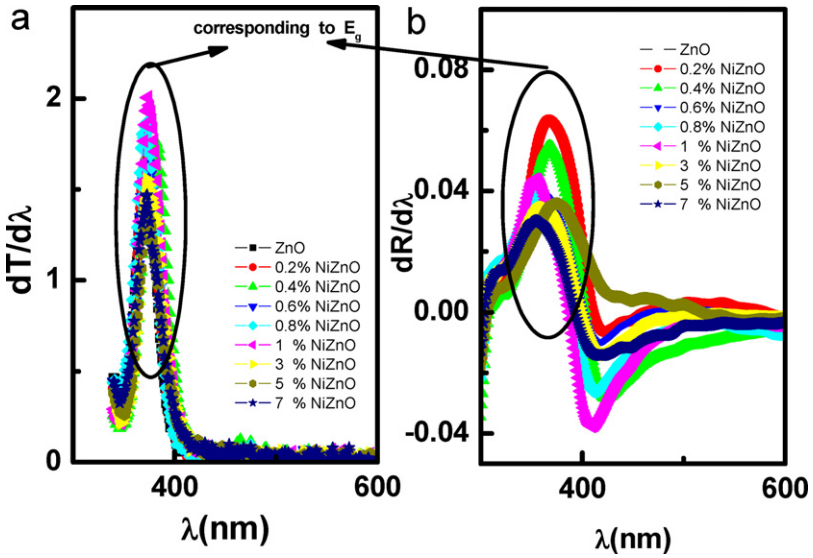

Fig. 5. (a) Plot of the first derivative of the transmittance, $dT/d\lambda$ vs. λ of undoped ZnO and Ni-doped ZnO. (b) Plot of spectral dependence of the first derivative of the reflectance, $dR/d\lambda$ of undoped ZnO and Ni-doped ZnO.

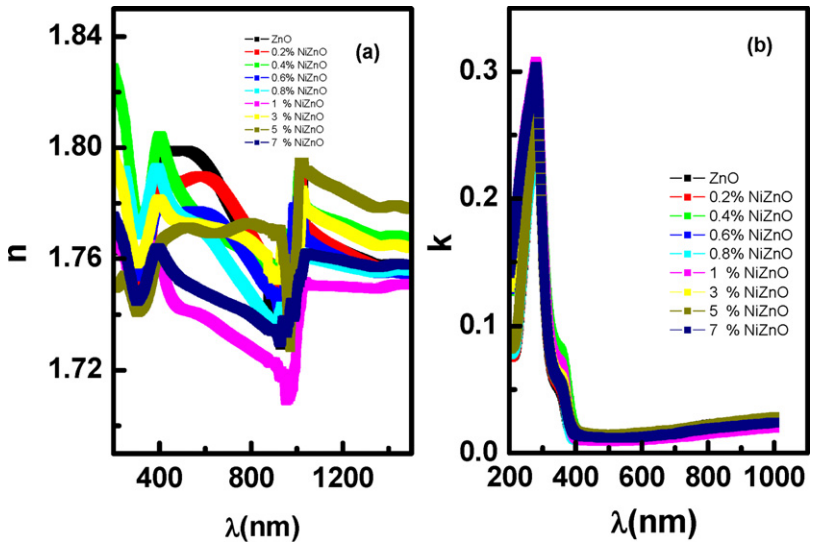

Fig. 6. (a) Plot of spectral dependence of refractive index of undoped ZnO and Ni-doped ZnO. (b) Plot of spectral dependence of absorption index of undoped ZnO and Ni-doped ZnO.

where A is an energy-independent constant and E_g is the optical band gap. This equation can be rewritten as:

$$\frac{d[\ln(\alpha h\nu)]}{d(h\nu)} = \frac{m}{h\nu - E_g} \tag{5}$$

The type of the optical transition can be obtained to find the value of m. The $d[\ln](\alpha h\nu)/d(h\nu)$ vs. $h\nu$ was plotted, as shown in Fig. 8. The peak at a particular energy value gives approximately the optical band gap E_g. The peak in Fig. 8 was found to be at $h\nu = E_g \approx 3.3$ eV as tabulated in Table 1 for ZnO and Ni-doped ZnO films. The values of $\ln(\alpha h\nu)$ vs. $\ln(h\nu - E_g)$ were plotted using the value of E_g to determine the m parameter and it was determined to be 1/2 from the slope of Fig. 9. In order to determine a more precise value of the optical band gap, we plotted $(\alpha h\nu)^2$ as a function of photon energy. This plot gives a straight line, as shown in Fig. 10. The optical band gap was determined by extrapolating the linear portion of the plot to $(\alpha h\nu)^2 = 0$. This suggests that the fundamental absorption edge of the film is formed by the indirect allowed transitions. The calculated value of the optical band gap for the ZnO and Ni-doped ZnO films was determined and is given in Table 1.

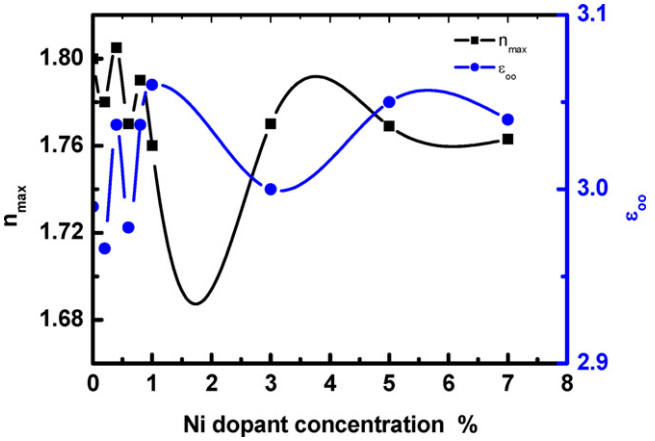

Fig. 7. Plot of n_{max} and ε_∞ vs. Ni dopant concentration %.

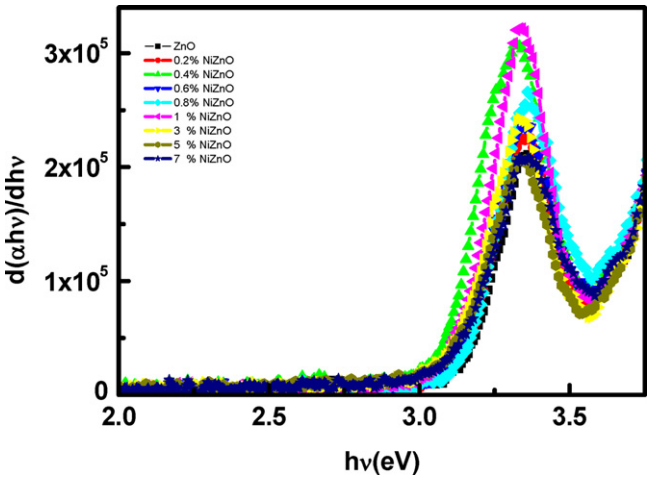

Fig. 8. Plot of photon energy dependence of $d(\alpha h\nu)/dh\nu$ of undoped ZnO and Ni-doped ZnO.

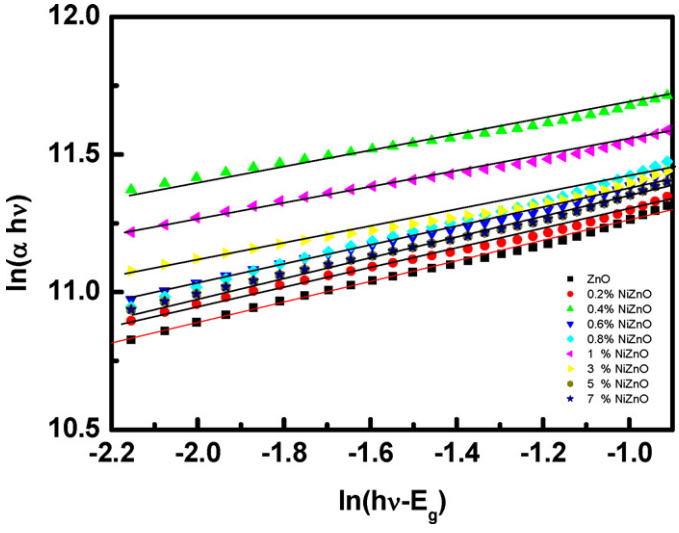

Fig. 9. Plot of $\ln(\alpha h\nu)$ vs. $\ln(h\nu - E_g)$ of undoped ZnO and Ni-doped ZnO.

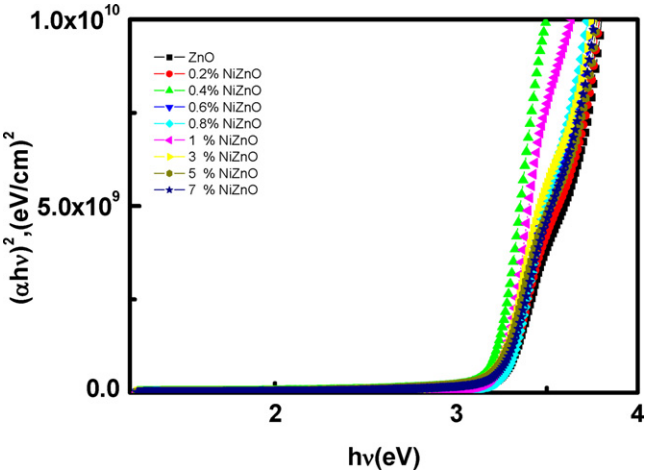

Fig. 10. Plot of photon energy dependence of $(\alpha h\nu)^2$ of undoped ZnO and Ni-doped ZnO.

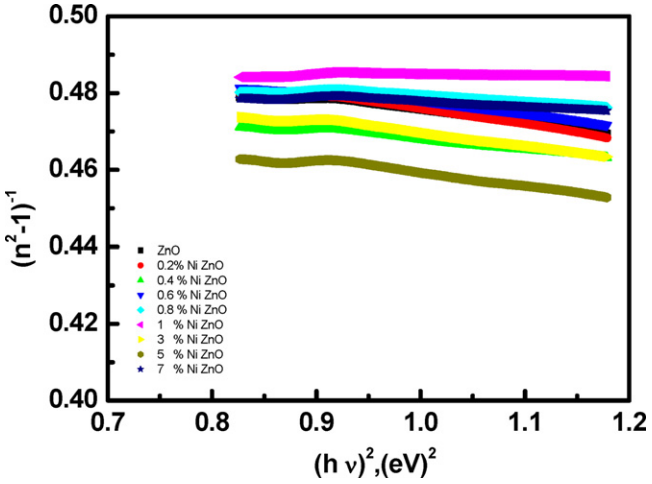

Fig. 11. Plot of $(n^2-1)^{-1}$ vs. $(h\nu)^2$ of undoped ZnO and Ni-doped ZnO.

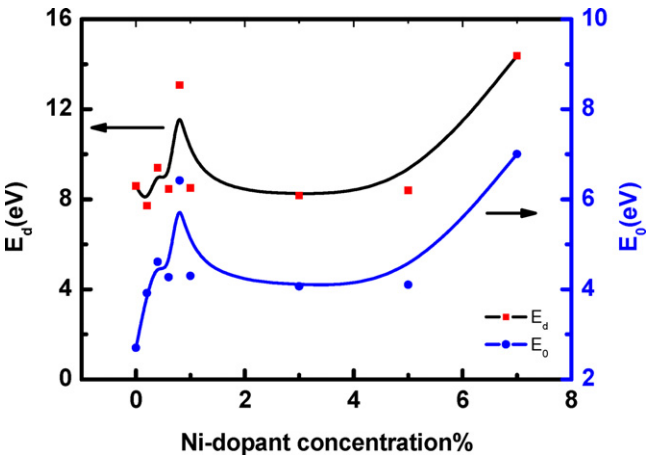

Fig. 12. Plot of E_d and E_0 vs. Ni dopant concentration %.

3.5. Refractive index dispersion behavior of the ZnO films

The dispersion plays an important role in the research for optical materials, because it is a significant factor in optical communication and in designing optical devices. The dispersion theory suggests that at the region of low absorption, the refractive index, n, is expressed by the single oscillator model [46,47]:

$$n^2 \leftrightarrows = 1 + \leftrightarrows \frac{E_d E_0}{E_0^2 - E^2} \quad (6)$$

where E is the photon energy, E_0 is the oscillator energy and E_d is the dispersion energy. The parameter E_d, which measures the intensity of the inter-band optical transition, does not depend significantly on the band gap. A plot of $(n^2-1)^{-1}$ vs. E^2 of the ZnO and Ni-doped ZnO films is shown in Fig. 11. It is clear that the refractive index decreases towards the longer wavelengths due to the influence of lattice absorption. The extrapolating of the linear part towards longer wavelengths which is the point of interception with the ordinate at $(h\nu)^2 = 0$ yields the value of the dielectric constant at higher wavelength (ε_∞). The obtained values of ε_∞ for ZnO and Ni-doped ZnO films were given in Table 2.

The values of E_d and E_0 were obtained from the slope $(E_d E_0)^{-1}$ and the intersection (E_0/E_d) obtained from extrapolation of the line to zero photo energy of Fig. 11. Fig. 12 shows the variation of E_0 and E_d with Ni dopant for ZnO and Ni-doped ZnO films. As observed, the values of E_0 and E_d have no regular change from undoped ZnO to 0.8% Ni doped film, after which there is a sharp increase for the values of E_0 and E_d by increasing the Ni% up to 5%, after which the values are decreased. This behavior is similar to the optical parameters with Ni doping concentration for ZnO.

The dispersion energy E_d, obeys the following empirical relationship [46,47]:

$$E_d = \beta N_c Z_a N_e \quad (7)$$

where N_c is the coordination number of the cation nearest-neighbor to the anion, Z_a is the formal chemical valency of the anion, β is the effective number of valence electrons per anion and β is a constant (0.37 ± 0.04) for covalently bonded crystalline and amorphous chalcogenides and 0.26 ± 0.04 eV for halides and most oxides that have ionic structure. Taking $N_c = 4, Z_a = 2, N_e = 8$ for ZnO [25,26], the β value values for ZnO and Ni-doped ZnO films were determined and are given in Table 2. As observed, the obtained values of β are less than the published for ZnO [46,47]. The ionic property is

Table 2
Dispersion parameters of undoped and Ni-doped ZnO films.

	n_{max}	ε_∞	β	ε_L	N/m^* (g^{-1} cm^{-3})	f(eV)^2
Ni content%						
0	1.81	2.99	0.134	3.15	3.76×10^{46}	23.19
0.2	1.78	2.96	0.120	3.16	4.65×10^{46}	30.22
0.4	1.80	3.03	0.147	3.18	3.48×10^{46}	43.33
0.6	1.80	2.97	0.132	3.14	3.81×10^{46}	36.08
0.8	1.77	3.03	0.204	3.10	1.52×10^{46}	83.90
1	1.76	3.06	0.133	3.08	2.33×10^{45}	34.25
3	1.78	3.00	0.127	3.18	7.76×10^{46}	33.21
5	1.77	3.05	0.131	3.23	4.40×10^{46}	34.44
7	1.76	3.05	0.209	3.11	1.30×10^{46}	100.59

most obvious for the Ni-doped ZnO films with concentration of Ni of about 0.8% and 7%, where $\beta = 0.204$ and 0.209, respectively.

There is an important parameter called the oscillator strength (f) as reported in [48] such that:

$$f = E_0 E_d \tag{8}$$

The oscillator strength for undoped ZnO and Ni-doped ZnO films was determined and is given in Table 2. As observed, the highest oscillator strength is for the 5% Ni-doped ZnO films.

The obtained data of the refractive index n can be analyzed to obtain the high-frequency dielectric constant via a procedure that describes the contribution of the free carriers and the lattice vibration modes of the dispersion [49]. The relation between the optical dielectric constant, ε, the wavelength, λ, and the refractive index is given by the following equation:

$$\varepsilon_1 = n^2 = \varepsilon_L - D\lambda^2 \tag{9}$$

where ε_1 is the real part of the dielectric constant, ε_L is the dielectric constant or (the high-frequency dielectric constant) and D is a constant depending on the ratio of carrier concentration to the effective mass; $D = e^2N/4\pi^2\varepsilon_0 m^* c^2$, where e is the charge of the electron, N is the free charge carrier concentration, ε_0 is the permittivity of free space, m^* is the effective mass of the electron and c is the velocity of light. Fig. 13 shows the relation between n^2 and λ^2 for the ZnO films. It is observed that the dependence of ε_1 on λ^2 is linear at longer wavelengths. It can be shown that the refractive index has an anomalous dispersion in the region of the high frequency. As the refractive index increases, there is also an increased of the absorption of electromagnetic radiation associated with an increase of the frequency. Furthermore, the refractive index becomes considerable high, when the frequency of the radiation crosses with the characteristic frequency of the electron. Hence, there is no propagation of electromagnetic radiation through the ZnO films. As shown in Fig. 13, the dependence of n^2 is linear at the longer wavelengths. The value of the lattice high frequency dielectric constant ε_L is determined from the intersection of the straight line with $\lambda^2 = 0$. Table 2 lists the values of ε_L and the ratio N/m^* for ZnO and Ni-doped ZnO films. The obtained values are in the order of 10^{46} cm^{-3} g^{-1}. It is clear from the obtained results that $\varepsilon_\infty < \varepsilon_L$, which can be attributed to the contribution of the free charge carrier.

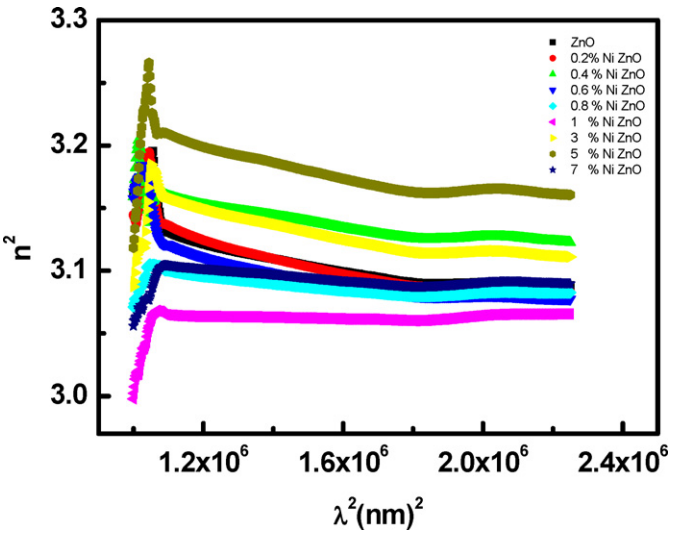

Fig. 13. Plot of n^2 vs. λ^2 of undoped ZnO and Ni-doped ZnO.

3.6. Dielectric characterization of the ZnO films

The complex refractive index $\hat{n} = n + ik$ and the dielectric function $\hat{\varepsilon} = \varepsilon_1 + i\varepsilon_2$ characterize the optical properties of any solid material. The real and imaginary parts of the complex dielectric constants are expressed as [50]:

$$\varepsilon_1(\omega) = n^2(\omega) - k^2(\omega), \tag{10}$$

$$\varepsilon_2(\omega) = 2n(\omega)k(\omega) \tag{11}$$

where ε_1 and ε_2 are the real and imaginary parts of the dielectric constant, respectively. The dependences of ε_1 and ε_2 on the photon energy are shown in Fig. 14 for the undoped ZnO and Ni-doped ZnO films. The real and imaginary parts follow different patterns and the values of the real part are higher than the imaginary part. The variation of the dielectric constant with photon energy indicates that some interactions between photons and electrons in the films are produced in this energy range. These interactions are observed in the shapes of the real and imaginary parts of the dielectric constant

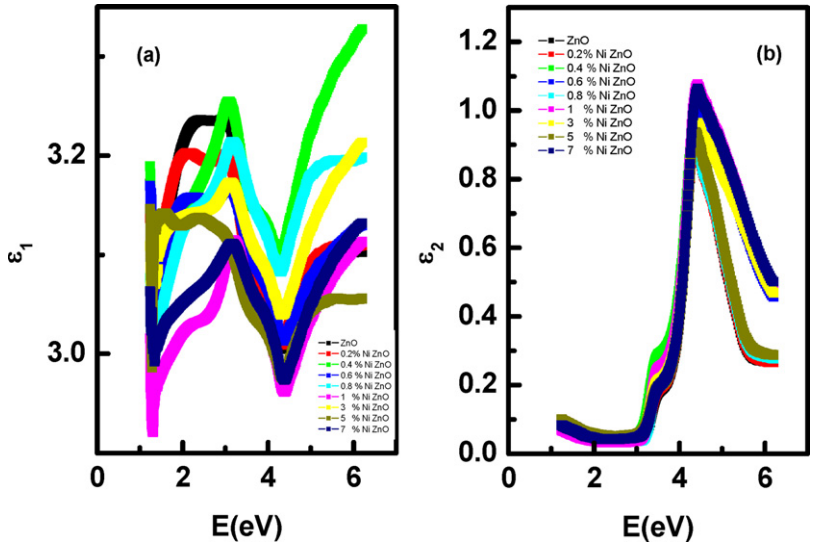

Fig. 14. (a) Plot of photon energy dependence of real dielectric constant of undoped ZnO and Ni-doped ZnO. (b) Plot of photon energy dependence of imaginary dielectric constant of undoped ZnO and Ni-doped ZnO.

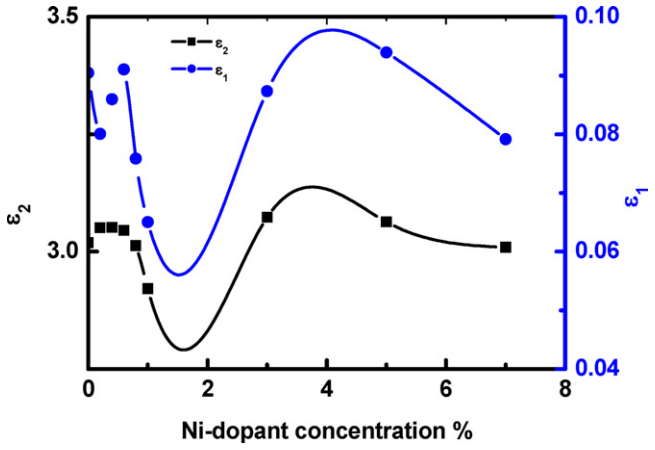

Fig. 15. Plot of ε_1 and ε_2 vs. Ni dopant of undoped ZnO and Ni-doped ZnO film.

and they cause formation of peaks in the dielectric spectra which depends on the material type.

Savvides [51] stated that assuming the conduction band states were constant; the increase in density of states would result in redistribution of valence band states. This, in turn, will cause the states from the top of the valence band to be pushed deep into the valence band with their contribution appearing at higher energies of $\varepsilon_2(\omega)$. Fig. 15 shows the variation of ε_1 and ε_2 for ZnO and Ni-doped ZnO films. As observed, the values of ε_1 and ε_2 have the same change for undoped ZnO to 1% Ni doped film after which there is an increase for the values of ε_1 by increasing the Ni% up to 5% after which the values are decreased in contradiction with ε_2.

The dissipation factor $\tan\delta$ is defined as the ratio of the power loss in a dielectric material to the total power transmitted through the dielectric, the imperfection of the dielectric. Most dielectrics have a low dissipation factor, a desirable property because it minimizes the waste of electrical energy as heat. The dissipation factor $\tan\delta$ can be calculated according to the following equation:

$$\tan\ \delta = \frac{\varepsilon_2}{\varepsilon_1} \tag{12}$$

The variation of $\tan\delta$ with $h\nu$ for undoped ZnO and Ni-doped ZnO films is shown in Fig. 16. It is found that the dissipation factor has a little change in the energy region and increases with increasing the photon energy when the photon energy is less than 3.4 eV. With an increase in the photon energy, a rapid increase in the dissipation factor in the photon energy range 3.4–4.4 eV is observed. On the other hand, the rapid decrease of the dissipation factor is observed when the photon energy increases larger than 4.5 eV for all samples.

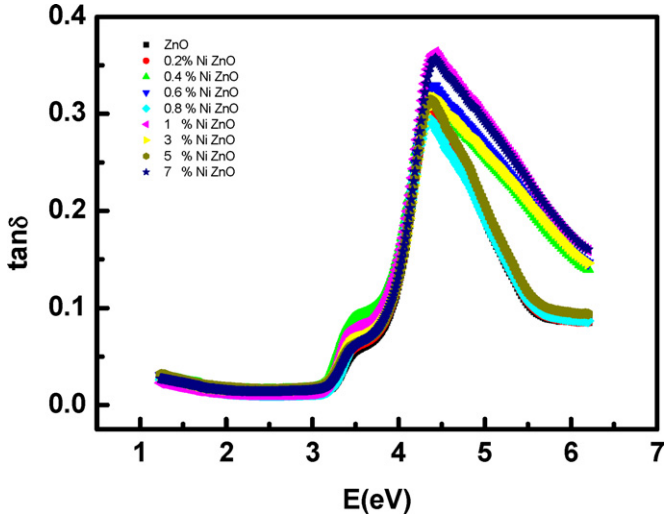

Fig. 16. Plot of photon energy dependence of $\tan\delta$ of undoped ZnO and Ni-doped ZnO.

4. Conclusions

Thin films of undoped ZnO and Ni-doped ZnO (0.2%, 0.4%, 0.6%, 0.8%, 1%, 3%, 5% and 7%) films were prepared by sol–gel spin coating process. The doping concentration of 5% Ni doped ZnO is proved to be optimum for Ni-doped zinc oxide thin films. According to AFM, all the films have a fiber network structure. The optical constants of the undoped and Ni doped ZnO films were characterized using spectrophotometric measurements. The refractive index of the as-deposited film is affected with Ni doping concentration. The Ni-doping affects the values of the calculated dispersion parameters such as oscillator energy, dispersion energy, and oscillator strength.

Acknowledgments

This work was supported by the Management Unit of Scientific Research Projects of Firat University (FÜBAP) (Project Number: 1947) and Global Research Network for Electronic Devices & Biosensors (GRNEDB) and KING Saud University.

References

[1] A.B. Moghaddam, T. Nazari, J. Badraghi, M. Kazemzad, Int. J. Electrochem. Sci. 4 (2009) 247.
[2] R. Baron, F.W. Campbell, I. Streeter, L. Xiao, R.G. Compton, Int. J. Electrochem. Sci. 3 (2008) 556.
[3] A. Bayandori Moghaddam, M. Kazemzad, M.R. Nabid, H.H. Dabaghi, Int. J. Electrochem. Sci. 3 (2008) 291.
[4] D.J. Milliron, S.M. Hughes, Y. Cui, L. Manna, J. Li, L.-W. Wang, A.P. Alivisatos, Nature 430 (2004) 190.
[5] D.C. Look, Mater. Sci. Eng. B 80 (2001) 383.
[6] J.J. Ding, H.X. Chen, S.Y. Ma, Physica E 42 (2010) 1861.
[7] L. Vayssieres, K. Keis, A. Hagfeldt, S.-E. Lindquist, Chem. Mater. 13 (2001) 4395.
[8] Z.W. Pan, Z.R. Dai, Z.L. Wang, Science 292 (2001) 1947.
[9] J.A. Rodriguez, T. Jirsak, J. Dvorak, S. Sambasivan, D.J. Fischer, J. Phys. Chem. B 104 (2000) 319.
[10] W.-C. Shin, M.-S. Wu, J. Cryst. Growth 137 (1994) 319.
[11] H.M. Huang, S. Mao, H. Feick, H. Yan, Y. Wu, H. Kind, E. Weber, R. Russo, P.D. Yang, Science 292 (2001) 1897.
[12] N.T. Hung, N.D. Quang, S. Bernik, J. Mater. Res. 16 (2001) 2817.
[13] N.F. Cooray, K. Kushiya, A. Fujimaki, D. Okumura, M. Sato, M. Ooshita, O. Yamase, Jpn. J. Appl. Phys. 38 (1999) 6213.
[14] R. Paneva, D. Gotchev, Sens. Actuators A: Phys. 72 (1999) 79.
[15] E. Topoglidis, A.E.G. Cass, B. Oregan, J.R. Durrant, J. Electroanal. Chem. 517 (2001) 20.
[16] L. Gao, Q. Li, W.L. Luan, J. Am. Ceram. Soc. 85 (2002) 1016.
[17] C.X. Xu, X.W. Sun, Appl. Phys. Lett. 83 (2003) 3806.
[18] P.X. Gao, Y. Ding, W. Mai, W.L. Hughes, C.S. Lao, Z.L. Wang, Science 309 (2005) 1700.
[19] Y. Fangli, H. Peng, Y. Chunlei, H. Shulan, L. Jinlin, J. Mater. Chem. 13 (2003) 634.
[20] T. Masui, M. Yamamoto, T. Sakuta, H. Mori, G. Adachi, J. Mater. Chem. 10 (2000) 353.
[21] K.X. Chen, H. Wang, J. Colloid Interface Sci. 330 (2009) 380.
[22] B.B. Lia, X.Q. Xiua, R. Zhanga, Z.K. Taoa, L. Chena, Z.L. Xie, Y.D. Zheng, Mater. Sci. Semicond. Proc. 9 (2006) 141.
[23] D. Wu, M. Yang, Z. Huang, G. Yin, X. Liao, Yunqing, J. Colloid Interface Sci. 330 (2009) 380.
[24] Y. Wang, X. Liao, Z. Huang, G. Yin, J. Gu, Y. Yao, Colloids Surf. A: Physicochem. Eng. Aspects 372 (2010) 165–171.
[25] K. Sato, H. Katayama-Yoshida, J. Appl. Phys. 40 (2001) 334.
[26] A. Korbecka, J.A. Majewski, Low Temp. Phys. 35 (2009) 53.
[27] J.H. Li, D.Z. Shen, J.Y. Zhang, D.X. Zhao, B.S. Li, Y.M. Lu, Y.C. Liu, X.W. Fan, J. Lumin. 122–123 (2007) 352.
[28] J.T. Prater, S. Ramachandran, A. Tiwari, J. Narayan, J. Electron. Mater. 35 (2006) 852.
[29] D. Karmakar, S.K. Mdaanl, R.M. Kadam, P.L. Paulose, A.K. Rajarajan, T.K. Nath, A.K. Das, I. Dasgupta, G.P. Das, Phys. Rev. B 75 (2007) 144404.
[30] C.W. Cheng, G.Y. Xu, H.Q. Zhang, Y. Luo, Mater. Lett. 62 (2008) 1617.
[31] S. Ghosh, P. Srivastava, B. Pandey, M. Saurav, P. Bharadwaj, D.K. Avasthi, D. Kabiraj, S.M. Shivaprasad, Appl. Phys. A 90 (2008) 765.
[32] C.J. Cong, J.H. Hong, Q.Y. Liu, L. Liao, K.L. Zhang, Solid State Commun. 138 (2006) 511.

[33] D.W. Wu, M. Yang, Z.B. Huang, G.F. Yin, X.M. Liao, Y.Q. Kang, X.F. Chen, H. Wang, J. Colloid Interface Sci. 330 (2009) 380.
[34] M.M. El-Nahass, A.A.M. Farag, A.A. Atta, Synth. Met. 159 (2009) 589.
[35] P.P. Banerjee, Proc. IEEE 73 (2005) 1859.
[36] T.H. Gfroerer, in: R.A. Meyers (Ed.), Encyclopedia of Analytical Chemistry, 2000, Copyright ©John Wiley & Sons Ltd.
[37] Z. Fang, Y. Wang, D. Xu, Y. Tan, X. Liu, Opt. Mater. 26 (2004) 239.
[38] V.S. Khomchenko, T.G. Kryshtab, A.K. Savin, L.V. Zavyalova, N.N. Roshchina, V.E. Rodionov, O.S. Lytvyn, V.I. Kushnirenko, V.B. Khachatryan, J.A. Andraca-Adame, Superlattice Microstruct. 42 (2007) 94.
[39] S. Ilican, Y. Caglar, M. Caglar, F. Yakuphanoglu, J. Cui, J. Alloys Compd. 490 (2010) 62.
[40] F. Yakuphanoglu, Opt. Mater. 29 (2006) 253–256.
[41] D.A. Minkov, J. Phys. D: Appl. Phys. 22 (1989) 1157.
[42] T. Fujii, H. Nishikiori, T. Tamura, Chem. Phys. Lett. 233 (1995) 424.
[43] S.K. Gagandeep, B.S. Lark, H.S. Sahota, Nucl. Sci. Eng. 134 (2000) 208.
[44] G. Kaur, K. Singh, B.S. Lark, H.S. Sahota, Radiat. Phys. Chem. 58 (2000) 315.
[45] G.K. Sandhu, K. Singh, B.S. Lark, L. Gerward, Radiat. Phys. Chem. 65 (2002) 211.
[46] S.H. Wemple, M. Didomenico, J. Phys. Rev. B 3 (1971) 1338.
[47] S.H. Wemple, M. Didomenico, J. Phys. Rev. B 7 (1973) 3767.
[48] S.H. Wemple, M. DiDomenico, J. Phys. Rev. Lett. 23 (1969) 1156.
[49] G.A. Kumar, J. Thomas, N. George, B.A. Kumar, P. Radhakrishnan, V.P.N. Nampoori, C.P.G. Vallabhan, J. Phys. Chem. Glasses 41 (2000) 89.
[50] A.A.M. Farag, I.S. Yahia, Opt. Commun. 283 (2010) 4310.
[51] N. Savvides, B. Window, J. Vac. Sci. Technol. A 3 (1985) 2386.